JACC: BASIC TO TRANSLATIONAL SCIENCE VOL. 10, NO. 5, 2025


ORIGINAL RESEARCH - PRECLINICAL

# Delayed miR-199a Administration After Myocardial Infarction Precludes Pro-Regenerative Effects

Gia Burjanadze, MD, PhD,[a,*] Nikoloz Gorgodze, MD, PhD,[b,*] Giovanni Donato Aquaro, MD,[c] Khatia Gabisonia, MD, PhD,[a] Lucia Carlucci, VD, PhD,[a] Manendra Pachauri, PhD,[d] Federico Turreni, MD,[e] Ilaria Secco, PhD,[f] Fabio Bernini, MS,[a] Lorena Zentilin, PhD,[d] Mauro Giacca, MD, PhD,[f,†] Fabio A. Recchia, MD, PhD[a,b,g,†]

## VISUAL ABSTRACT

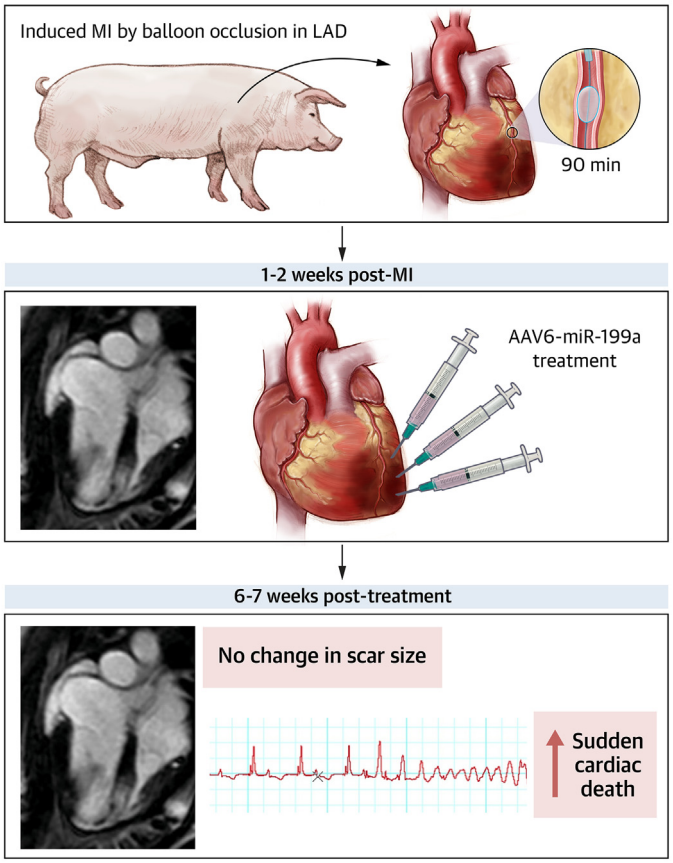


Burjanadze G, et al. JACC Basic Transl Sci. 2025;10(5):634-649.

## HIGHLIGHTS

- **Different from its high effectiveness when administered early after myocardial infarction, the AAV6 vector carrying the pri-miRNA-199a gene fails to stimulate cardiac regeneration when administered at 1 or 2 weeks later in pigs.**
- **Despite therapeutic ineffectiveness, the delayed administration of AAV6-*pri-miRNA-199a*, similar to the early administration after myocardial infarction, is associated with sudden death in the long term.**
- **Therefore, for clinical translation, it appears mandatory to administer miR-199a early after myocardial infarction and through a modality that does not involve permanent expression from a viral vector.**

From the [a]Interdisciplinary Research Center "Health Science," Scuola Superiore Sant'Anna, Pisa, Italy; [b]Aging + Cardiovascular Discovery Center, Lewis Katz School of Medicine, Philadelphia, Pennsylvania, USA; [c]Academic Radiology, Department of Surgical, Medical and Molecular Pathology and Critical Care Medicine, University of Pisa, Pisa, Italy; [d]Molecular Medicine Laboratory, International Centre for Genetic Engineering and Biotechnology (ICGEB) and Department of Medical Sciences, Faculty of Medicine,

ISSN 2452-302X https://doi.org/10.1016/j.jacbts.2024.12.014

## SUMMARY

miR-199a carried by adeno-associated virus serotype 6 (AAV6) proved cardioreparative in a pig model when administered early after myocardial infarction (MI). To test whether the therapeutic efficacy of miR-199a is maintained when its administration is delayed, AAV6-miR-199a or a control AAV6 were injected 1 or 2 weeks after MI. Scar mass and cardiac contractile performance parameters were not significantly different between AAV6-miR-199a–treated and AAV6-control pigs. Nonetheless, most AAV6-miR-199a–treated pigs died from sudden death at 40 to 52 days after vector administration. For clinical translation, it appears mandatory to administer miR-199a early after MI and through modalities other than permanent expression from a viral vector. (JACC Basic Transl Sci. 2025;10:634–649) 

## ABBREVIATIONS AND ACRONYMS

**AAV6** = adeno-associated virus serotype 6

**AUC** = area under the curve

**cMRI** = cardiac magnetic resonance imaging

**LGE** = late gadolinium enhancement

**LV** = left ventricular

**MI** = myocardial infarction

**miRNA** = microRNA

**MRI** = magnetic resonance imaging

**PCR** = polymerase chain reaction

**PES** = programmed electrical stimulation

**W1** = week 1

**W2** = week 2

Molecular therapies for the regeneration of infarcted hearts harness the action of cell cycle regulators to boost the proliferation of cardiomyocytes and other cell types.[1-6] They do not require laborious processes of stem cell isolation, characterization, and ex vivo expansion and resemble classic pharmacologic therapies more closely. Among the biological molecules capable of driving cardiac cell proliferation, microRNAs (miRNAs) deserve special attention because their potential therapeutic value has been documented by studies in small and large animal models. Several miRNAs that tune cardiomyocyte proliferation have been identified by both transcriptional profiling in pre- and postnatal hearts,[7] and high-throughput screenings of synthetic miRNA mimic libraries[8] (reviewed in Braga et al[9]). One class of these pro-proliferative miRNAs is expressed in embryonic stem cells and is active during the early stages of embryonic development, including miRNAs in the miR-302∼367 and its related miR-290∼295 clusters.[10,11] A second class comprises miRNAs that regulate the cell cycle in cancer cells and other cell types, and their prototypes are found in the miR-17∼92 cluster.[12,13] A third class includes a series of individual miRNAs that were identified through large, high-throughput screenings for neonatal cardiomyocyte proliferation, among which are miR-199a-3p, miR-590-3p, and the primate-specific miR-1825.[8] These miRNAs exert their pro-proliferative action by activating the Hippo signaling pathway positive effector YAP1 (Yes-associated protein),[14] a major modulator of proliferation and chromatin accessibility in the fetal heart,[15] and by regulating actin polymerization in cardiomyocytes.[14]

Based on the pro-proliferative effect of miR-199a-3p in both mouse and rat neonatal cardiomyocytes[8] and its capacity to stimulate cardiac regeneration after myocardial infarction (MI) in mice when administered using either an adeno-associated virus serotype (AAV)9 vector[8] or by lipofection,[16] we tested this miRNA in a large animal model of MI.[17] Using an AAV6 vector, we delivered to pig hearts[17] the gene coding for the miR-199a *pri-miRNA*, from which both the miR-199a-5p and miR-199a-3p miRNAs are generated, the latter only exerting a pro-regenerative effect. Multiple intramyocardial injections of AAV6-miR-199a in the peri-infarct area during the first 20 minutes of reperfusion after 90 minutes of coronary occlusion resulted in a marked reduction in scar size and significant improvement in functional parameters 1 month later.[17] Morphologic and functional amelioration correlated with an increased number of cardiomyocytes that were positive for Ki67 (a proliferation marker) or for incorporated bromodeoxyuridine (an S-phase marker) as well as cardiomyocytes that displayed phosphorylated histone H3 (a marker of G2/M cell cycle transition).[17] Consistently, at 1 month after treatment, the hearts showed markedly reduced

University of Trieste, Trieste, Italy; [e]Emergency Department and Internal Medicine, Santa Maria della Stella Hospital, Orvieto, Italy; [f]School of Cardiovascular and Metabolic Medicine & Sciences and British Heart Foundation Centre of Research Excellence, King's College London, London, United Kingdom; and the [g]Institute of Clinical Physiology of the National Research Council, Pisa, Italy. *These authors have equally contributed to this work. †These authors jointly supervised this work.

The authors attest they are in compliance with human studies committees and animal welfare regulations of the authors' institutions and Food and Drug Administration guidelines, including patient consent where appropriate. For more information, visit the Author Center.

Manuscript received September 11, 2024; revised manuscript received December 13, 2024, accepted December 16, 2024.

**FIGURE 1 Experimental Protocols**

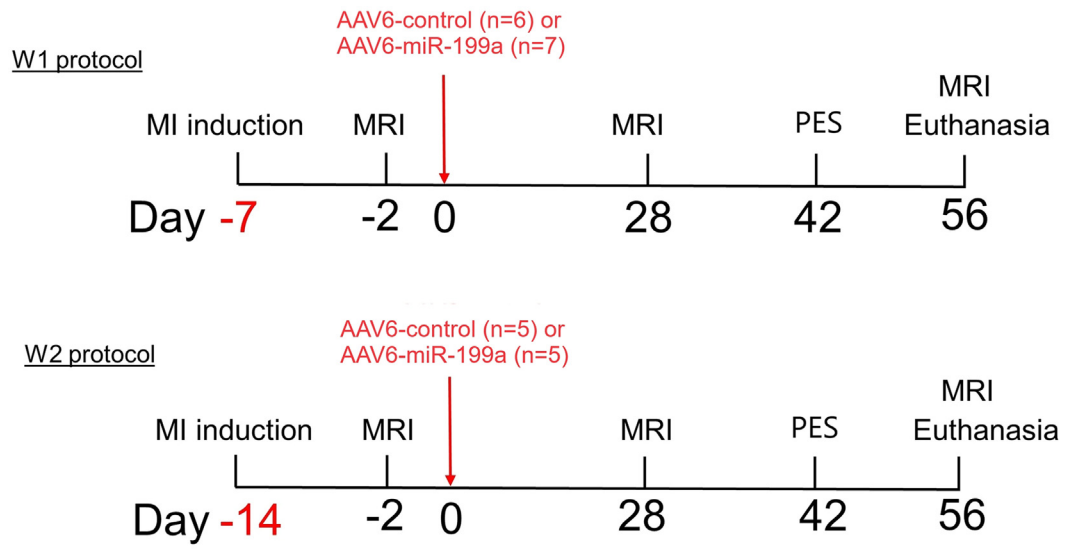


Pigs were randomly assigned to a W1 or W2 protocol and further randomly assigned to administration of adeno-associated virus serotype 6 (AAV6)-control or AAV6-miR-199a. MI = myocardial infarction; MRI = magnetic resonance imaging; PES = programmed electrical stimulation; W1 = week 1; W2 = week 2.

scarring and increased remuscularization.[17] All these functional, histologic, and molecular observations were in agreement at also showing bona fide miRNA-induced cardiac regeneration after MI in pigs.

Our prior results left a few questions unaddressed, in particular whether the administration of AAV6-miR-199a at later time points after MI would also be effective at stimulating a regenerative response, which would pave the way to using a miRNA-based therapy in patients with more established cardiac injury. In addition, in our previous study, we also observed cardiac arrhythmias and sudden death in several miR-199a-treated pigs, which occurred only at >6 weeks after vector administration. The electrophysiological substrate for such unexpected lethal events, not preceded by any other clinical sign, remained unknown. In the present study, we aimed to provide answers to these outstanding questions by testing the cardioreparative effects of AAV6-miR-199a administered at 1 and 2 weeks after MI and performing electrophysiological studies after vector administration.

## METHODS

**EXPERIMENTAL PROTOCOL.** The protocol was approved by the Italian Ministry of Health (no. 76/2014 PR), conformed to Italian law (D.lgs. 26/2014), and complied with all institutional and national requirements for the care and use of laboratory animals. Thirty-eight castrated male farm pigs (3-4 months old, weighing 28-32 kg) underwent percutaneous coronary catheterization to induce MI. MI was induced by 90-minute occlusion of the left anterior coronary artery by coronary balloon inflation. Pigs with MI were randomly divided into 4 groups receiving an intramyocardial injection of AAV6-miR-199a or AAV6 vector carrying an empty polylinker (AAV6-control) after 10 to 15 minutes of reperfusion: 2 groups were administered AAV6 at week 1 after MI (groups W1: AAV6-control and AAV6-miR-199a) and 2 groups were administered AAV6 at week 2 after MI (groups W2: AAV6-control and AAV6-miR-199a) to test possible time-dependent changes in the efficacy of miR-199a. Cardiac magnetic resonance imaging (MRI) was performed at baseline (2 days before treatment to quantify the area at risk) and 28 days after treatment (Figure 1). A set of animals underwent MRI also on day 56, just before they were killed and their tissue collected. At day 40 after treatment, pigs belonging to the W1 group were subjected to an electrophysiological study. An additional group of 6 sham-operated animals underwent percutaneous catheterization in the same manner, but the balloon was not inflated.

The protocol followed the 2010/63/EU directive for animal handling. The experimental protocols were designed to maximally limit the animal perception of pain and discomfort during the procedures.

Experiments were carried out by highly specialized operators. Because of single-pen housing, physiological functions and general well-being were closely monitored. Space between the bars separating pens permitted visual and olfactory contact between animals. Environmental enrichment was also implemented, and animals walked on nonslip floor. Animals had access to unlimited clean water in pens.

**PRODUCTION AND PURIFICATION OF RECOMBINANT AAV VECTORS.** The generation of an AAV plasmid expressing the *hsa-miR-199a pri-miRNA* under the control of the constitutive cytomegalovirus promoter was described previously.[17] The plasmid pZac2.1 (Gene Therapy Program, Penn Vector Core, University of Pennsylvania, Philadelphia, Pennsylvania, USA) was used to produce AAV6 vectors. HEK293T cells were co-transfected with the plasmid vector together with the packaging plasmid pDP6 (PlasmidFactory). Cells for AAV production were free from mycoplasma contamination. Viral stocks were obtained by polyethylene glycol precipitation and 2 subsequent CsCl2 gradient centrifugations. Titration of AAV viral particles was performed by real-time polymerase chain reaction (PCR) quantification of the number of packaged viral genomes, as described previously[18]; the viral preparations yielded titers comprising between $1.3 \times 10^{13}$ and $3.3 \times 10^{13}$ viral genomes per milliliter.

**CLOSED-CHEST MI INDUCTION.** Pigs were sedated with an intramuscular injection of a cocktail of 4 mg/kg tiletamine hydrochloride and 4 mg/kg zolazepam, intubated, and mechanically ventilated with positive pressure. Inhalation anesthesia was maintained with a mixture of 2.5% to 3% sevoflurane dissolved in 40% air and 60% oxygen. Electrocardiogram, heart rate, and arterial pressure were constantly monitored. Before starting a coronary angiography, pigs received antibiotics (amoxicillin/clavulanic acid: 1000/200 mg intravenously) and analgesics (ketorolac: 30 mg/mL intravenously). Thirty minutes before coronary occlusion, 4.3 mg/kg of amiodarone in 500 mL of 5% glucose was intravenously given to prevent arrhythmias.

Ultrasound-guided arterial access was obtained under sterile conditions by applying the Seldinger technique, and an 8-F introducer sheath (Avanti; Cordis) was inserted into the right femoral artery. Systemic, nonfractionated heparin was injected intravenously (150 IU/kg) through the percutaneous sheath. Under fluoroscopic guidance (Philips BV Pulsera; Philips Medical Systems), a 7-F multiaortic curve 4.5 guiding catheter (Cordis) with an angled guidewire (0.35 inch/150 cm J/ST; Terumo) was advanced up to the origin of the left main coronary artery. Coronary angiograms were obtained in the 0° anteroposterior projection to assess the detailed anatomy of the left anterior descending coronary artery and its diagonal branches. After withdrawing the angled guidewire, a J-curve coronary guidewire was introduced into the left anterior descending coronary artery (0.014 inch/175 cm, Reflex; Cordis). An over-the-wire coronary balloon of an appropriate diameter (Apex 2.5-3.0 mm/10 mm; Boston Scientific) was then advanced into the left anterior descending coronary artery and positioned below the first diagonal branch, just above the origin of the second diagonal branch. The balloon was inflated for 90 minutes, and the artery occlusion was verified by intracoronary infusion of the radiocontrast agent (Ultravist-370; Bayer Schering Pharma) through the guiding catheter. Coronary occlusion was confirmed by the presence of ST-segment elevation and ventricular arrhythmias, which were more pronounced within 30 to 45 minutes after coronary occlusion.

For cases of ventricular tachycardia, compromising hemodynamics, or ventricular fibrillation, external cardiac massage was started with a frequency of 100 per minute. External defibrillations (360 J) were often necessary, and amiodarone (100 mg intravenous bolus) and adrenaline (1 mg per intravenous push) were administered between the electrical discharges at 3- to 5-minute intervals. A further 10 mL of heparinized saline (50 IU/kg) was administered before balloon deflation and removal. To avoid hematoma formation, vigorous compressions were applied on the site of introducer insertion for at least 10 minutes or until the hemorrhage stopped. The artificial ventilation was gradually reduced until tracheal tube removal, and the animals were taken back to the cages for full recovery from anesthesia.

**OPEN-CHEST AVV6 INJECTION.** At W1 or W2 after MI, the animals were sedated, anesthetized, and monitored as described above; placed in a right lateral position; and subjected to open-chest surgery. A thoracotomy was performed in the left fourth intercostal space, and the pericardial sac was opened to expose the heart. The animals were randomized in 2 groups, those receiving $2 \times 10^{13}$ control AAV6 (AAV6-control) or those receiving $2 \times 10^{13}$ AAV6-miR-199a. The viral particles were suspended in 2 mL of phosphate-buffered saline and delivered by 20 direct intramyocardial injections equally spaced along the border zone (100 μL per injection), which was visually identified as the margin of the ischemic myocardium (pale and hypokinetic compared with the normally perfused myocardium). Some of the injection sites were tagged with colored epicardial stitches to detect

and sample postmortem the underlying myocardial tissue for histologic analysis. Sham animals underwent open-chest surgery without any intramyocardial injections.

**CARDIAC MRI.** Cardiac MRI (cMRI) was performed 2 days before (baseline) and 4 weeks and 8 weeks after AAV administration. Pigs were sedated with a cocktail of 4 mg/kg tiletamine hydrochloride and 4 mg/kg zolazepam hydrochloride injected intramuscularly, and light anesthesia was maintained by continuous intravenous infusion of propofol (30-40 μg/kg/min) at spontaneous respiration. Pigs were placed in the right lateral position with the heart at the isocenter of the MRI scanner. Electrocardiogram was monitored continuously. Images were acquired with a clinical 1.5-T scanner (Signa Excite HD; GE Medical Systems), using a non-breath-hold, electrocardiogram-gated, multi-NEX steady-state free precession pulse sequence (fast imaging using steady-state acquisition).[19] The heart was scanned along 2 long-axis views (vertical and horizontal) and with a set of short-axis views covering the entire left ventricle from the atrioventricular valve plane to the apex. The following parameters were used: field of view 30 cm, slice thickness 8 mm, no gap between each slice, repetition time 3.7 ms, echo time 1.6 ms, views for segment 2, flip angle 45°, bandwidth 125 Hz, 30 phases, matrix 224 × 224, reconstruction matrix 256 × 256, NEX 3, free breathing.

Tagging-MR images were acquired with an electrocardiography-gated, segmented K-space, fast gradient recalled echo pulse sequence with spatial modulation of magnetization to generate a grid tag pattern. Nonselective radiofrequency pulses separated by spatial modulation of magnetization-encoding gradients allowed tag separation of 10 mm. Three sets of short axes at basal-, middle-, and apical-level views were acquired with a grid of tags lines with 45° and 135° angulation. The number of views per phase was optimized based on heart rate. The following parameters were used: field of view 30 cm, slice thickness 8 mm, no gap between each slice, repetition time 8 ms, echo time 4.3 ms, flip angle 15°, bandwidth 31 Hz, 30 phases, matrix 192 × 192, reconstruction matrix 256 × 256, NEX 3.

To identify the scar and quantify the extension of postinfarction fibrosis, delayed enhanced images were acquired in 2-dimensional, T1-weighted, segmented inversion recovery gradient echo sequence 5 to 10 minutes after administration of gadoteric acid (0.2 mmol/kg intravenously) in short- and long-axis views corresponding to those of cine cMRI. The following parameters were used: field of view 30 mm, slice thickness 8 mm, no gap between each slice, repetition time 4.6 ms, echo time 1.3, flip angle 20°, matrix 224 × 192, reconstruction matrix 256 × 256, number of excitations 3.

**MR IMAGES ANALYSIS.** MR images were analyzed in a blinded manner under the supervision of a III-level European Association of Cardiovascular Imaging MRI-accredited cardiologist, using a commercially available research software package (Mass 6, Medis Medical Imaging). To detect postinfarction fibrosis and determine its size, the short-axis stack of images of the left ventricle was first assessed visually for the presence of late gadolinium enhancement (LGE), as shown in **Figure 2**. The quantification of LGE was then performed on all LGE-positive studies by manually adjusting a grayscale threshold to define areas of visually identified LGE. These areas were then summed to generate the total volume of LGE and expressed as a proportion of total left ventricular (LV) myocardium.[20] The infarct areas were also analyzed using the full-width half-maximum method[21] to differentiate the dense infarct core from the heterogeneous gray zone, as previously described.[22] The infarct core was defined as an area with a signal intensity > 50% of the maximal signal intensity of the enhanced myocardium. The gray zone of the infarct periphery was defined as the myocardium with a signal intensity value higher than the peak value of the remote myocardium but lower than 50% of the peak value of the high signal intensity myocardium. Finally, the infarction core and the gray zone were quantified as a percentage of the total myocardium and as a percentage of the total infarct size.

Functional parameters describing global (end-diastolic volume and end-systolic volume, ejection fraction) and regional (LV wall thickening) LV function were measured as previously described.[22,23] LV endocardial and epicardial borders were manually traced on all short-axis cine images at the end-diastolic and end-systolic frames to determine the end-diastolic and end-systolic volumes, respectively, as well as ejection fraction and cardiac mass (**Figure 3**). The same software was used to calculate LV wall thickening. In brief, the left ventricle was divided in 6 slices orthogonal to the LV long axis, and each slice was divided into 6 equal circumferential segments (**Figures 4A and 4B**). The inferoseptal segment at the connection of the right ventricle with the left ventricle was defined as a reference point for the ventricular segmentation. Six segments were plotted to generate the curve and subsequently calculate the area under the curve (AUC)[24] (**Figures 4D and 4E**).

**FIGURE 2** **miR-199a Delivery Did Not Affect MI Scar Size**

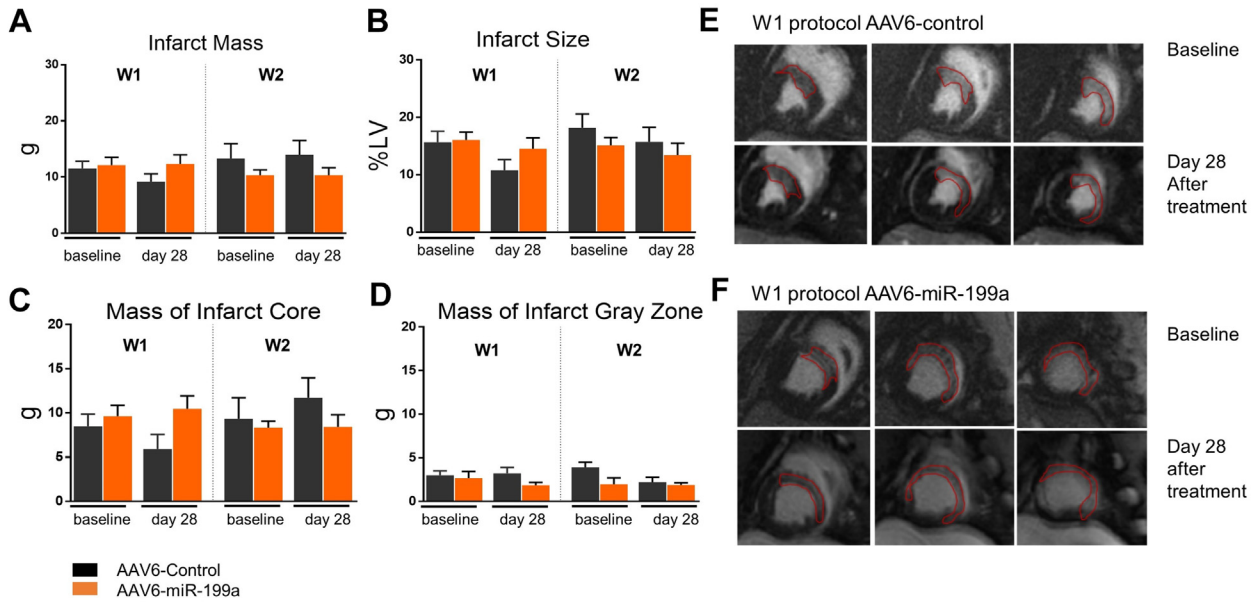


Infarct mass (A), size (B), infarct core (C), and infarct gray zone (D) (calculated from late gadolinium enhancement [LGE]-positive regions as a percentage of the left ventricle) at 2 days before (baseline) and 28 days after adeno-associated virus (AAV) administration in AAV serotype 6 (AAV6-control (5-6) and AAV6-miR-199a (5-7)), pigs. Data are mean ± SEM. Two-way analysis of variance. (E and F) LGE cardiac magnetic resonance images (from base to apex) are shown from 2 representative pig hearts of the W1 protocol to compare AAV6-control (E) with AAV6-miR-199a (F) at 2 and 28 days after MI. The infarct area is highlighted in red; the corresponding original images without highlight are shown in Supplemental Figure 1. Abbreviations as in **Figure 1**.

The analysis of tagged cardiac images was performed using a custom software based on a previously published method[25] (the software code can be provided upon request via email to the corresponding author). The 2-dimensional maximal radial strain was evaluated along short-axis LV slices (basal, middle, and apical), divided into 8 equal circumferential segments, starting from the reference point of the ventricular segmentation (**Figure 4C**). The radial strain values, obtained for each segment, were plotted to generate curves, as in the case of LV wall thickening (**Figures 4F and 4G**, respectively), and, subsequently, the AUC was calculated to integrate all values along the LV circumference (scheme in **Figures 4F and 4G**).

**ELECTROPHYSIOLOGICAL STUDIES.** Forty days after AAV6 injection (ie, 2 days before the end of the sixth week after gene transfer), pigs from the W1 protocol were premedicated, anesthetized, and held on mechanical respiration as described for the other procedures. The electrophysiological study (ie, programmed electrical stimulation [PES]) was performed using an integrated electrophysiology stimulator and amplifier (GE CardioLab Electrophysiology Recording Systems). An approximately 10-cm-long incision was made along the ventral side, and the external jugular vein was isolated from the surrounding tissues. Then, after inserting an 8-F introducer sheath (Avanti; Cordis) into the right external jugular vein, a quadripolar catheter (Biosense Webster) was advanced through it into the right ventricular cavity under x-ray fluoroscopic guidance. The PES protocol was performed according to clinical standards.[26-28] Briefly, the right ventricle was stimulated at twice the diastolic threshold, up to 5 mA and up to a 2-ms duration, delivering an 8-beat pacing drive train (**Figures 5F and 5G**) with a cycle length of 600 ms; a premature extrastimulus (S1) was introduced, gradually shortening the coupling intervals of the train and the extrastimulus (train-S1) until sustained monomorphic ventricular tachycardia or ventricular fibrillation were provoked or ventricular refractoriness was achieved. If sustained ventricular tachycardia or ventricular fibrillation were not induced, a second extrastimulus (S2) was introduced while train-S1 was held just above the ventricular refractory period. S1 and S2 were progressively reduced until arrhythmias

**FIGURE 3 Late miR-199a Delivery Does Not Improve Global Cardiac Function**

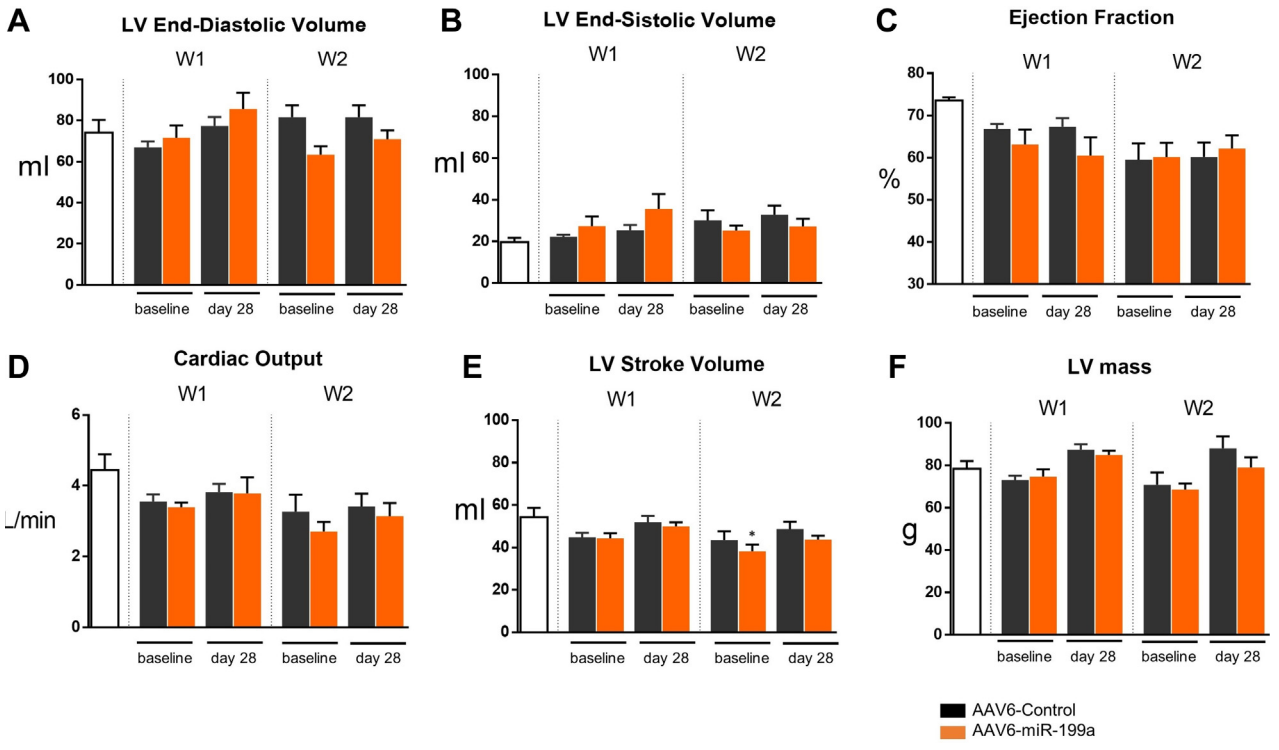


(A) Left ventricular (LV) end-diastolic volume ($P = 0.079$), (B) LV end-systolic volume ($P = 0.19$), (C) LV ejection fraction ($P = 0.062$), (D) cardiac output ($P = 0.072$), (E) LV stroke volume ($P = 0.023$), and (F) LV mass ($P = 0.005$) measured by cardiac MRI in noninfarcted controls and infarcted pigs 2 days before (baseline) and 28 days after injection of adeno-associated virus serotype 6 (AAV6-control (5-6) and AAV6-miR-199a (5-7)). Data are mean ± SEM. *$P < 0.05$ vs sham. Two-way analysis of variance with Bonferroni post-hoc correction. See detailed results in Supplemental Table 1 for LV stroke volume and Supplemental Table 2 for LV mass. Abbreviations as in **Figure 1**.

were provoked or refractoriness was reached. In the absence of arrhythmias, triple extrastimuli (S1-S2-S3) were delivered similarly. As a next step, the single (S1), double (S1-S2), and triple (S1-S2-S3) extrastimuli were delivered similarly with a faster drive train (500 ms and 400 ms). Finally, the burst ventricular stimuli were applied. Biphasic DC cardioversion/defibrillation was used to stop ventricular tachycardia or ventricular fibrillation and restore the sinus rhythm. After completing the procedure, the surviving animals were brought back to their cages.[29]

**DEATH OF THE PIGS AND HEART SECTIONING.** At the end of the study, animals were anesthetized and killed by injecting 10% KCl to stop the heart in diastole. The excised hearts were sectioned through 4 horizontal planes, and each section was then subdivided into subsections for further histologic and molecular analyses, as shown in Supplemental Figure 1. In brief, each heart was sectioned into four 1-cm-thick slices, starting from the apex toward the base. Each slice was then divided into 4 to 9 regions (indicated by letters). In all quantifications, we considered at least 8 sectors of the 4 heart sections. Sectors T, I, and D corresponded to the infarct border zone, where the vectors were administered, whereas sector L was considered representative of the remote zone, because it was on the same plane but on the opposite position (posterior) relative to sector H. Each region was then divided into 2 pieces (for RNA analysis and histology) by a transversal cut to keep both the endocardial and pericardial borders visible in each piece. For all quantifications, the same regions were chosen in animals injected with either control or miR-199a vectors.

**HISTOLOGIC ANALYSIS.** The collected hearts were rinsed with phosphate-buffered saline, weighed, and cut into slices as shown in Supplemental Figure 1A. The slices were then fixed in 10% formalin, embedded in paraffin, and further cut into 4-μm sections and collected on glass slides. The sections were

**FIGURE 4** Cardiac Regional Wall Motion

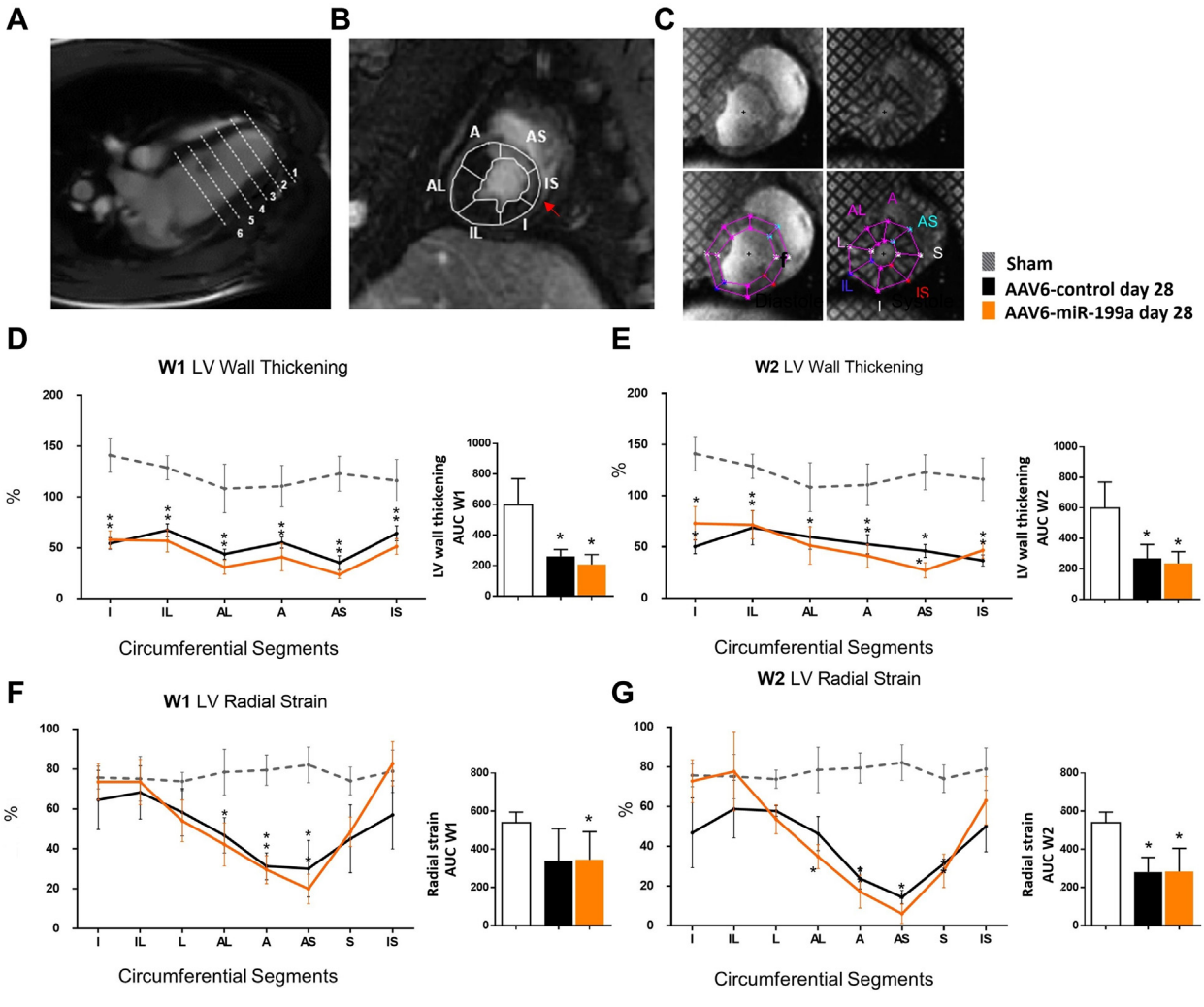


Left ventricular (LV) wall thickening long (A) and short-axis (B) cardiac MRI (cMRI) segmentation scheme for regional wall motion evaluation. The red arrow indicates the reference point (ie, the LV inferoseptal segment at the connection of the right ventricle). (C) cMRI tagging segmentation scheme for LV strain evaluation. (D and E) Six-segment curves generated from LV segmental wall thickening of W1 (D) and W2 (E) protocol groups with their corresponding AUCs quantified in arbitrary units (5-6). (F and G) Eight-segment curves generated from LV radial strain in W1 (F) and W2 (G) protocol groups and their corresponding AUCs (4-6). Data are mean ± SEM *$P < 0.05$ vs sham. One-way analysis of variance with Bonferroni post hoc correction. AAV6 = adeno-associated virus serotype 6; AUC = area under curve; circumferential segments: I = inferior; IL = inferolateral; AL = anterolateral; A = anterior; AS = anteroseptal; IS = inferoseptal; other abbreviations as in Figure 1.

deparaffinized and rehydrated. Hematoxylin and eosin staining was performed using a standard protocol. The slides were dehydrated, mounted, and then observed under an optical microscope (Leica DM750). Masson's trichrome staining (Bioptica) was performed according to standard procedure and analyzed for the morphology and the extent of fibrosis. Immunofluorescence staining was performed on deparaffinized and rehydrated sections. Antigen retrieval was performed by boiling samples in sodium citrate solution (0.1 M, pH 6.0) for 20 minutes. Sections were allowed to cool and permeabilized for 20 minutes in 1% Triton X-100 (Sigma) in phosphate-buffered saline, followed by blocking in 1% bovine serum antigen (Sigma). Sections were then stained overnight at 4 °C with the following primary antibodies diluted in blocking solution, recognizing the following antigens: sarcomeric α-actinin (Abcam ab9465, 1:250), cardiac troponin I (Abcam ab8295, 1:250), Ki67 (Cell Signaling 9129S, 1:500), GATA 4

**FIGURE 5 Electrophysiological Substrate Evaluation**

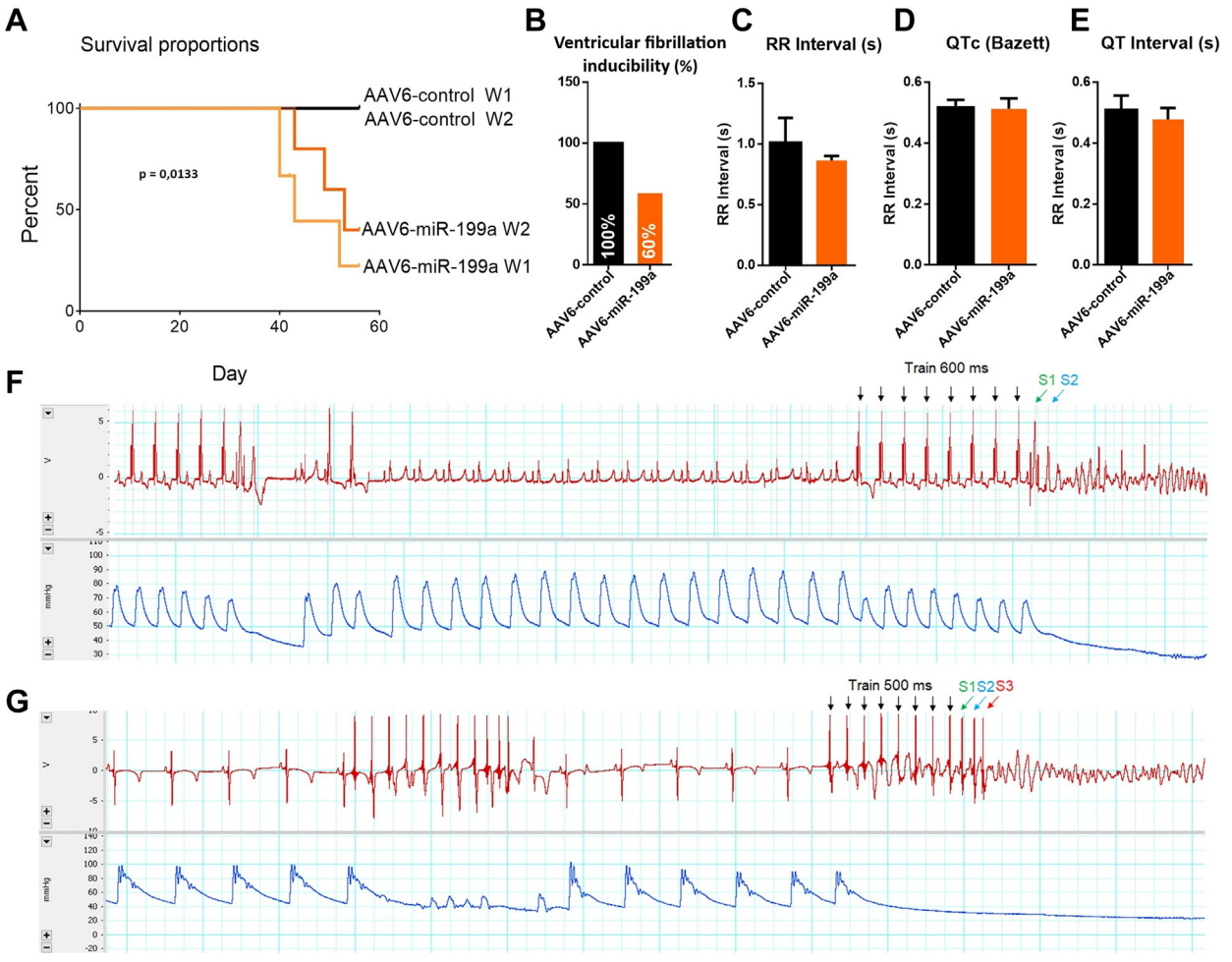


(A) Kaplan-Meier curve depicting survival rates in pigs treated 2 weeks and 1 week after MI (AAV6-control (5-6) and AAV6-miR-199a (5-7)); $P < 0.05$ vs control animals). No differences were found in miR-199a treated and control pigs in terms of ventricular fibrillation induction (B), the time between two successive R-waves of the QRS signal on the electrocardiogram (C), QT interval (D), and QTc (corrected QT) (E) (1 week protocol; (AAV6-control n = 5 and AAV6-miR-199a n = 5). Data are mean ± SEM; unpaired *t* test. (F) Representative case of ventricular fibrillation induction with the PES protocol in a AAV6-miR-199a pig following the stimulation of the train 600 ms (black arrows), S1-420 ms (green arrow), and S2-350 ms (blue arrow). (G) Representative case of ventricular fibrillation induction with the PES protocol in a AAV6-control following the stimulation with coupling intervals of the train 500 ms (black arrows), S1-320 ms (green arrow), S2-320 ms (blue arrow), S3-240 ms (red arrow). Abbreviations as in Figures 1 and 2.

(Abcam ab84593, 1:200), connexin 43 (Abcam ab11370, 1:500). Sections were washed with phosphate-buffered saline and incubated for 2 hours with the respective secondary antibodies conjugated with Alexa Fluor 555 or Alexa Fluor 647 (Life Technologies).

To measure the cardiomyocyte cross-sectional area, lectin wheat germ-agglutinin-Alexa Fluor 647 (ThermoFisher Scientific) was diluted 1:200 in phosphate-buffered saline and incubated for 20 minutes. Slides were mounted with mounting medium containing DAPI (Abcam) to counterstain the nuclei.

For each animal, at least 8 sectors belonging to all 4 heart slices and sections were considered. Histologic analysis was performed by researchers blinded to experimental groups on at least 20 images at 10× magnification.

**IN SITU HYBRIDIZATION.** Four-micron-thick tissue sections from formalin-fixed, paraffin-embedded tissue samples were cut using a microtome. The sections were then deparaffinized by xylene and rehydrated with graded ethanol solutions. Proteinase K treatment demasked the miRNAs, allowing probes to

hybridize with the miRNA sequence. The miRCURY LNA miRNA detection probes (nonmammalian hapten digoxigenin-labeled from Qiagen, catalogue number 339112 YD0061541 O-BEG, product sequence 5'-3' /5DiGN/TMCCMTGTGCAGACTACTGT /3DiG _N/) were applied to the tissue sections, which were incubated at 52 °C for 1 hour. Stringent washes at 52 °C removed unbound probes. The anti-digoxigenin Fab fragments conjugated with the enzyme alkaline phosphatase were incubated for 1 hour. Later, chromogenic substrates (4-nitro-blue tetrazolium and 5-bromo-4-chloro3'-indolylphosphate) were applied for 2 hours. In this step, alkaline phosphatase converted the soluble substrates 4-nitro-blue tetrazolium and 5-bromo-4-chloro3'-indolylphosphate into a water- and alcohol-insoluble, dark blue 4-nitro-blue tetrazolium-5-bromo-4-chloro3'-indolylphosphate precipitate, which was observed under a bright-field microscope.

**RNA ISOLATION AND QUANTIFICATION.** Total RNA, including the small RNA fraction, was isolated from pig tissue fragments using the miRNeasy Mini Kit (Qiagen), according to the manufacturer's instructions. DNase treatment was performed during RNA isolation according to the manufacturer's protocol. For miR-199a-3p quantification, total RNA was reverse transcribed using a miRCURY LNA PCR synthesis kit (Qiagen), and quantitative reverse transcriptase PCR was performed with predesigned miRCURY LNA PCR primer sets (Qiagen) and miRCURY LNA SYBR Green master mix according to the manufacturer's instructions. miRNA expression was normalized based on the expression levels of 5S rRNA.

**STATISTICAL ANALYSIS.** Data are presented as the mean ± SEM unless otherwise indicated. Statistical analysis was performed using commercially available software (GraphPad Prism 9.5.1 [733]). Data were first checked for normal distribution, and then differences among groups were compared by 1-way or 2-way analysis of variance followed by Bonferroni's post-hoc test for multiple pairwise comparisons. When the comparisons included only 2 groups, we used the unpaired *t* test or Welch's *t* test depending on the equality of variances. For survival analysis, we generated Kaplan-Meier survival curves, followed by the log-rank test to compare groups. The AUC was obtained using the trapezoidal rule, and statistical comparisons were performed by 1-way or 2-way analysis of variance. The association between 2 continuous variables was assessed using the Pearson correlation coefficient. For all statistical analyses, $P < 0.05$ was considered statistically significant.

## RESULTS

**INFARCT SIZE.** Twenty-three of 38 pigs survived after the acute phase of MI or the surgery for AAV intramyocardial injection. The resulting sample size for each experimental groups was as follows: W1 AAV6-control, n = 6; W1 AAV6-miR-199a , n = 7; W2 AAV6-control , n = 5; and W2 AAV6-miR-199a , n = 5. LV scar assessment was performed using cMRI based on LGE. Both at baseline and at 1 month after treatment, the gadolinium-retaining region, defined as either infarct mass (gr) or size (% LV), was not significantly different between AAV6-control and AAV6-miR-199a ($P = 0.32$ and $P = 0.12$, respectively). Representative LGE cMR images of 4 cross-sectional planes of hearts of the W1 protocol at baseline and 28 days after treatment are shown in **Figure 2**. The infarct region included a core fibrotic area and a surrounding gray zone comprising a mixture of viable myocardium and fibrotic regions, which also did not differ between groups ($P = 0.18$ and $P = 0.20$, respectively).

**CARDIAC MORPHOLOGY AND FUNCTION.** Morphologic and functional changes, also measured with cMRI, were consistent with the lack of significant cardiac repair in the miR-199a-treated groups. No significant differences were found between the AAV6-control and AAV6-miR-199a groups, both in the W1 and W2 protocols, in terms of cardiac volumes and global systolic function (Supplemental Tables 1 and 2, **Figures 3A to 3E**; please see respective *P* values in the figure legend). There was a significant difference between groups in terms of indices of regional ventricular function, that is, wall thickening ($P < 0.001$), radial strain ($P < 0.001$), and relative AUC ($P < 0.032$), in both protocols, mainly because of differences between sham and infarcted groups but not between the 2 infarcted groups (**Figure 4**). Detailed post-hoc analyses for segmental wall motion parameters can be found in Supplemental Tables 3 to 5. Actual values of the key data elements are provided in Supplemental Table 6.

**ELECTROPHYSIOLOGICAL STUDY.** We started our study with the W2 group. It was clear, after the first few pigs, that the AAV-miR-199a administration was not effective when injected at 2 weeks after MI but still caused sudden death; hence, we decided to shorten the MI treatment window, and so we started in parallel with the W1 group, in which we also tested cardiac electrical stability. PES was performed in 5 pigs included in the W1 protocol for AAV6-miR-199a and 5 AAV6-control pigs. The RR interval, QT duration, and heart rate-corrected QT (QTc; Bazett's

formula) were not different between the 2 groups. Animals from the AAV6-miR-199a group showed higher, yet not significant, resistance to multiple extrastimuli with short coupling periods: Ventricular fibrillation was induced in 100% of AAV6-control pigs compared with 60% of AAV6-miR-199a pigs. No sustained monomorphic ventricular tachycardia was found in the AAV6-miR-199a group or in controls.

**DEATH RATE.** All pigs injected with AAV6-control survived until the end of the protocol (56 days after treatment). All 12 pigs receiving AAV6-miR-199a also survived up to week 40. However, 8 of them (3 in the W2 protocol and 5 in the W1 protocol) died suddenly at 40 to 52 days in the absence of preceding clinical signs $P = 0.013$) (**Figure 5A**).

**HISTOLOGIC AND MOLECULAR ANALYSES.** A group of animals (7 and 4 in the W1 and W2 protocols, respectively) was tested for expression of the mature miRNA-199a-3p in the infarct and injected border zones 8 weeks after AAV6 vector injection (**Figure 6A**). We found robust expression of miR-199a-3p in the animals that had received AAV6-miR-199a at both W1 and W2 after MI compared with the control group ($P = 0.033$ for W1 and $P = 0.041$ for W2). It consisted of an average of 10.9-fold (SEM, ±1.1) and 14.2-fold (SEM, ±7.0) endogenous to miR-199a-3p in the W2 and W1 protocols, respectively (**Figure 6C**). Individual values for each of the analyzed sections in 1 animal are shown in **Figure 6B**. These levels of overexpression are in line with those found in our previous study, when the same vector was administered immediately after MI,[17] and confirm the ability of AAV vectors to sustain expression of the transgenes over a long period of time.

Hematoxylin and eosin staining was performed on the paraffin-embedded tissue sections obtained according to the sectioning scheme shown in **Figure 6A**. The vast majority of the analyzed sections in the infarct border zones of the animals treated with AAV6-miR-199a did not show any unusual phenotype compared with untreated infarcted animals (representative images in **Figure 6D**). There was no difference in cardiomyocyte cross-sectional area between treated and control pigs ($P = 0.65$ for W1 and $P = 0.61$ for W2) (Supplemental Figures 2A and 2B), consistent with our results on LV wall thickening. In only 2 treated animals, we could detect a few clusters of small cells in the infarct border zone in 2 different sections (sections 58A and 59S) (**Figure 6E**) that were injected with AAV6-miR-199a. These rare clusters included a small number of cells and were isolated and occupied an area no larger than 1 $mm^2$ in a whole tissue section of no <150 $mm^2$. Several cells in these clusters were positive for Ki67, a marker indicating an active cell cycle state, and for GATA4, which is a marker of early myogenic development (Supplemental Figure 2C). Although the clusters were sporadic and smaller, and thus unlikely to correlate with the occurrence of possible deadly arrhythmias, these results confirm that AAV-mediated persistent expression of miR-199a in the infarcted heart is associated with the presence of proliferating cell clusters with an early myoblast phenotype similar to our previous study.[17]

Finally, we sought to co-localize, in the AAV6-miR-199a-treated animals, the areas of vector transduction by in situ RNA hybridization and the levels and organization of connexin-43-positive intercalated disc junctions. The results for 1 representative animal (of 4 treated and 2 controls analyzed) are shown in Supplemental Figure 3. AAV-mediated miRNA expression was clearly detectable in cardiomyocytes in the infarct and infarct border zone areas. The levels of transduction were quite nonhomogeneous, also as a consequence of the different extent of tissue damage. We detected an inverse correlation between the levels of connexin-43 and those of AAV-expressed miR-199a, with less-intense staining and less-organized junctions in the areas that expressed high levels of the vector RNA transgene (r: -0.266, $P = 0.019$) (Supplemental Figure 3D for quantification).

## DISCUSSION

The present results indicate that an AAV6 vector expressing the *miR-199a pri-miRNA* gene is not effective at stimulating cardiac regeneration when administered at 1 or 2 weeks after MI in pigs. This is different from our previous results, which showed cardiomyocyte proliferation and clinically relevant cardiac regeneration when the same dose of vector was administered within the first 20 minutes of reperfusion after 90 minutes of coronary occlusion.[17] Healing from MI is a dynamic process that starts with inflammation and necrosis and approximately 1 week later evolves into a stage when fibrosis predominates.[30] During the first few days after MI, the necrotic tissue is cleaned up by macrophages with proteinases that degrade the intercellular matrix. Although this may free up room for newly formed cardiomyocytes,[31] during the following fibrotic phase the injured area is invaded by myofibroblasts from the surrounding myocardium and the production of pro-collagen drastically increases. This later phase is also characterized by elevated levels of matrix proteins that play important structural and signaling

**FIGURE 6** **Histologic and Molecular Analyses**

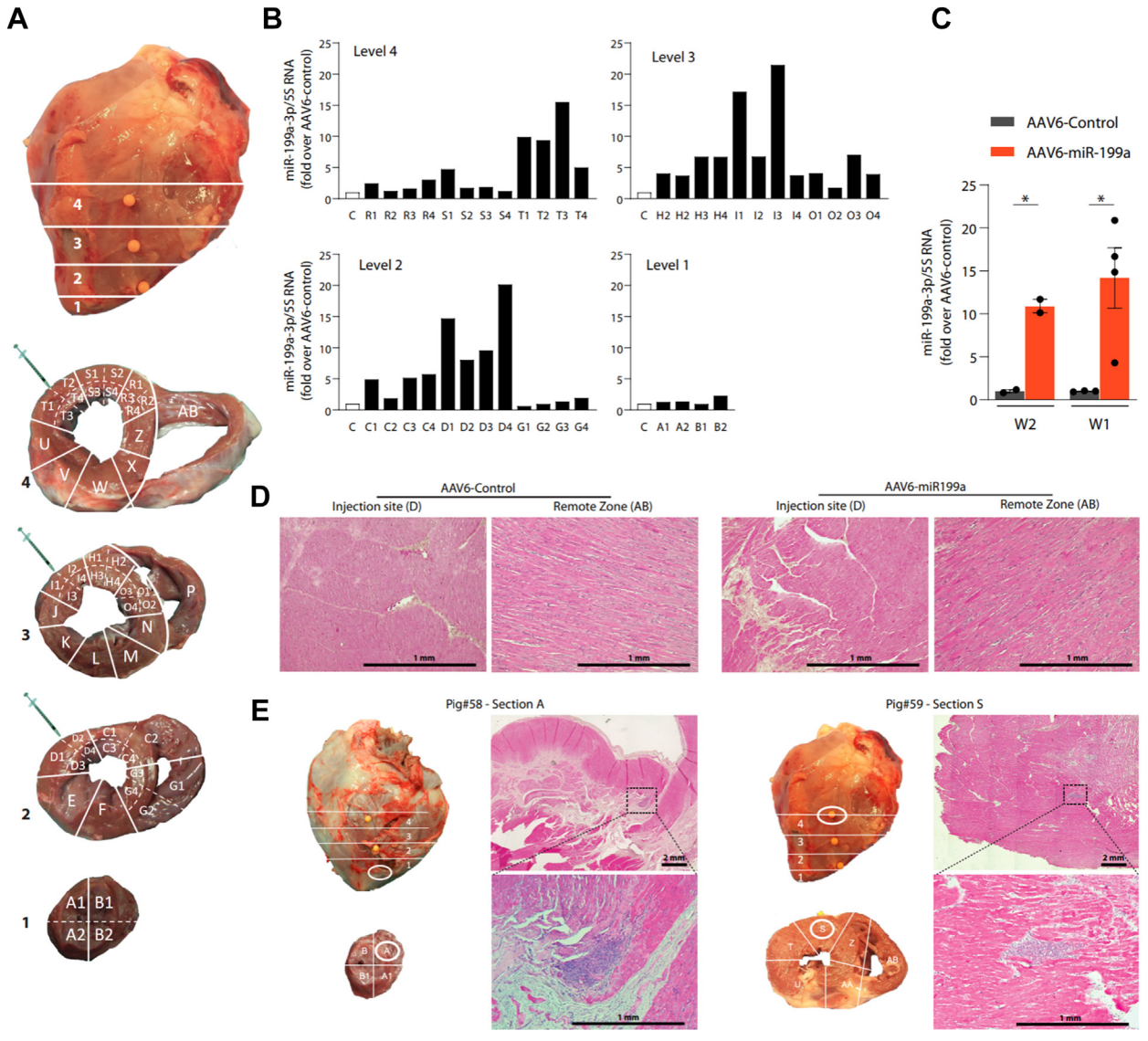


Systematic assessment of miR-199a-3p expression after AAV6-mediated transduction. (A) Schematic representation of pig heart sectioning for histologic and molecular studies. Four 1-cm-thick transversal slices were cut starting from the base to the apex (1-4). Each slice was subsequently divided into 2 to 9 regions, each 1 labeled with a capital letter, and then into additional subregions (letters plus numbers) for targeted molecular and histologic analyses. Sectors T, I, and D correspond to the infarct border zone, where the vectors were administered, whereas sector L was considered representative of the remote zone. Injection and infarct border segments for each slice were divided into smaller fragments (dashed lines) to accurately assess the levels of expression of the transgene at 56 days after transduction. (B) Real-time polymerase chain reaction quantification of mature miR-199a-3p expressed as fold change over endogenous levels (assessed in AAV6-control pigs) in the indicated regions for a representative animal. (C) Average expression levels of miR-199a-3p in the treated animals. Each data point represents an individual animal, averaging the highest levels detected in each subsegmented region. Three to 4 per sample. Data are mean ± SEM. *$P < 0.05$, unpaired $t$ test with Welch's correction.
(D) Hematoxylin & eosin staining of paraffin-embedded tissue sections in pigs injected with AAV6-miR-199a or AAV6-control. The pictures show representative images from the infarct border zone, which was injected, and a remote area. No apparent differences were detected in any analyzed sections taken from the treated pigs, except for the 2 sections shown in E. (E) Macroscopic picture of the only 2 sections in which small cell clusters were identified from 2 animals injected with AAV6-miR-199a. These sections were stained with hematoxylin & eosin and observed at 2 different magnifications.

roles in scar formation.[30,32-34] Such processes contribute to maintain ventricular integrity, scar compaction, and stability, hence preventing wall aneurism and rupture,[30,35] but they also create a disadvantageous milieu for proliferating cardiomyocytes. Consistent with these observations, other studies have shown that an attempt at tissue healing by spontaneously proliferating cardiomyocytes occurs immediately after MI in both rodents[36] and humans.[37] We can envisage that the expression of miR-199a is able to amplify the transient proneness of cardiomyocytes to proliferate immediately after MI, while this window of permissivity is closed at later times, during infarct healing process, when the fibrotic response predominates. Consistent with this conclusion, our original studies testing AAV6-miR-199a delivery at a very early stage of MI had already shown that the proliferation of cardiomyocytes had already ended 12 days after treatment, despite the continuous expression of the miRNA.[17]

These observations do not preclude the efficacy of other attempts at inducing endogenous cardiomyocyte proliferation as a mean to achieve cardiac regeneration at later times after MI. In species that regenerate their organs, such as zebrafish, heart regeneration is nevertheless preceded by extensive scar formation.[38] In the adult mouse heart, cardiomyocyte proliferation itself is a main driver for the resolution of scars, because fibrotic mouse hearts can still regenerate if the pro-proliferative YAP transcriptional cofactor is activated long after infarction.[39] Thus, although miR-199a may be effective only when administered early after coronary occlusion and reperfusion, other pro-proliferative treatments, including alternative miRNAs identified by our and others' screenings,[8,40] are worth testing under the same experimental conditions of the present study, long after MI.

The beneficial effects of miR-199a on post-MI cardiac recovery were lost when viral vector administration was delayed, and nonetheless most pigs still died suddenly at 6 to 7 weeks after AAV administration, possibly because of ventricular fibrillation, as we have previously recorded this lethal arrhythmia by implanted miniature electrocardiogram recorders (Medtronic) in pigs treated with AAV6-miR-199a.[17] On the other hand, PES, the standard test for ventricular arrhythmia susceptibility used in human patients, ruled out higher inducibility of ventricular fibrillation in miRNA-199a-treated hearts compared with the control group. PES induced ventricular fibrillation in 100% of the control pigs without preceding ventricular tachycardia, likely because of the aggressive stimulation protocol used. These findings seem to confirm that PES, although the best available choice for clinical assessments, is not an effective predictor of sudden cardiac death.[41,42] Another important aspect to be considered is that deadly cardiac events have never been observed in mice delivered with AAV-miRNA-199a.[8] Moreover, cardiac electrophysiology in pigs is characterized by differences relative to humans and other mammals.[43]

It is interesting that the long lag time between treatment and sudden death remained the same, no matter if AAV6-miRNA-199a was delivered during the period immediately after ischemia/reperfusion[17] or weeks after MI, as tested in the current study. What could be the reason for such possible arrhythmogenic effect occurring so long after vector administration? Our recent work in a different setting showed that transgene expression from AAV vectors starts a few hours after injection in infarcted hearts.[44] Therefore, the delayed lethal episodes are an unlikely consequence of the lag between vector administration and miRNA expression. In our previous study, we attributed this adverse effect to the continuous, pro-proliferative effect of miR-199a causing the formation of clusters of poorly differentiated myoblast cells interspersed among myocardial fibers.[17] In the present study, these infiltrating cell clusters were not detected in most cardiac sections we analyzed from the AAV6-miR-199a–treated animals (clusters of cells were only present in the 2 sections shown in **Figure 6E**). Thus, it appears highly unlikely that this occurrence could be linked to the development of arrhythmias.

The observation that the areas showing higher AAV RNA expression were those in which expression of connexin-43 was lower can have at least 3 explanations. First, it could reflect a true effect of the miRNA on connexin-43 levels. We consider this possibility unlikely, because neither connexin-43 mRNA levels nor connexin-43 protein localization in the intercalated discs were altered on miRNA expression in our previous studies.[3] A second possibility is that the reduced connexin-43 levels were a consequence of the uneven levels of transduction, because the vectors only target cardiomyocytes and were administered in the infarct border zone, in which the extent of tissue damage is highly variable and cardiomyocytes are less tightly connected. A third explanation relates to the possibility that the miRNA, although not directly reducing connexin-43 expression, could induce partial cardiomyocyte dedifferentiation, which in the short term would be required for cardiomyocyte proliferation but in the long term, because of the continued expression from AAV

vectors, could become detrimental by impeding proper electrical coupling of cardiomyocytes, hence favoring the occurrence of possible arrhythmias. Further experiments are required to discern among these possibilities.

**STUDY LIMITATIONS.** One limitation of our study, which could be considered among the hypothetical causes of the observed sudden death, is the use of AAV vectors expressing the *pri-miRNA* for miR-199a, which is processed inside cardiomyocytes to eventually yield the mature miRNA duplex. Both miRNA strands of the duplex can then be used by the endogenous RISC machinery. Therefore, not only the desired miRNA is produced (in this case, the pro-proliferative miR-199a-3p), but also the miRNA encoded by the complementary pre-miRNA stem-loop strand. In our previous experiments, both miR-199a-3p and miR-199a-5p were naturally generated by the same amount,[17] with the latter being known to exert undesirable effects in the heart.[45-48]

Different from our previous study,[17] we did not perform experiments to assess the presence of proliferating cardiomyocytes at 12 days after AAV6-miR-199a administration. However, because of this limitation, we cannot rule out that there could be a burst in cardiomyocyte cell cycle when AAV was administered 1 or 2 weeks after infarction. Our MRI data on scar size and cardiac function indicate no adequate regeneration in the infarct border zone. Another limitation is the missing comparison between male and female pigs, yet the present study compares directly with our previous one on AAV-miR-199a, also performed in castrated male pigs only.[17]

## CONCLUSIONS

The present results indicate that, for clinical translation, it appears mandatory to administer miR-199a-3p early after MI and through a modality that does not involve the permanent expression of pre-miRNA from a viral vector. Available evidence already indicates that synthetic miRNA mimics, including miR-199a-3p, are effective when administered by lipofection.[10,13,16,49] More studies in preclinical large animal models are warranted to test this alternative approach. In this respect, an appealing possibility for future clinical development is the use of lipid nanoparticles obtained through the SNALP (Stable Nucleic Acid Lipid Particles) technology.[50]

## FUNDING SUPPORT AND AUTHOR DISCLOSURES

This work was supported by the European Research Council Advanced Grant 787971 "CuRE," British Heart Foundation Programme Grant RG/19/11/34633, and the National Center for Gene Therapy and Drugs based on RNA Technology, PNRR, Italy, to Dr Giacca and grants 825670 "CardioReGenix" and 874764 "REANIMA" from the European Commission Horizon 2020 programme to Drs Recchia and Giacca. Dr Giacca is founder, consultant, member of the board, and equity holder in Forcefield Therapeutics, Heqet Therapeutics, and Purespring Therapeutics and is named as an inventor in patents on the use of microRNAs for cardiac regeneration. All other authors have reported that they have no relationships relevant to the contents of this paper to disclose.

**ADDRESS FOR CORRESPONDENCE:** Dr Fabio A. Recchia, Institute of Clinical Physiology, The National Research Council, Via Giuseppe Moruzzi, 1, 56124 Pisa, Italy. E-mail: fabio.recchia@ifc.cnr.it.

## PERSPECTIVES

**COMPETENCY IN MEDICAL KNOWLEDGE:** Despite its appealing characteristics, no miRNA-based therapy for cardiac diseases has yet achieved clinical approval. A marked cardioreparative capacity of miR-199a carried by AAV vectors (AAV6) was demonstrated previously in a clinically relevant model of infarcted pig heart, yet this therapy needs refinements to prevent possible lethal arrhythmias in the long term.

**TRANSLATIONAL OUTLOOK:** Using the pig model of MI, the present study tested whether a delayed administration of AAV6-miR-199a could be equally effective, while devoid of long-term severe side effects. That was not the case, because AAV6-miR-199a proved ineffective as a therapeutic agent while still being associated to sudden death in the long term. These results, although negative, provide important preclinical indications for a correct path toward the possible use of a powerful proreparative molecule such as miRNA-199a in human patients. It appears mandatory to administer miR-199a early after MI and through a modality that does not involve the permanent expression of pre-miRNA from a viral vector. More studies are warranted to test miRNA mimics carried by lipid nanoparticles.

## REFERENCES

**1.** Salama ABM, Gebreil A, Mohamed TMA, Abouleisa RRE. Induced cardiomyocyte proliferation: a promising approach to cure heart failure. *Int J Mol Sci*. 2021;22(14):7720. https://doi.org/10.3390/ijms22147720

**2.** Hashimoto H, Olson EN, Bassel-Duby R. Therapeutic approaches for cardiac regeneration and repair. *Nat Rev Cardiol*. 2018;15(10):585–600.

**3.** Bersell K, Arab S, Haring B, Kuhn B. Neuregulin1/ErbB4 signaling induces cardiomyocyte proliferation and repair of heart injury. *Cell*. 2009;138(2):257–270.

**4.** Mohamed TMA, Ang Y-S, Radzinsky E, et al. Regulation of cell cycle to stimulate adult cardiomyocyte proliferation and cardiac regeneration. *Cell*. 2018;173(1):104–116.

**5.** Mahmoud AI, Kocabas F, Muralidhar SA, et al. Meis1 regulates postnatal cardiomyocyte cell cycle arrest. *Nature*. 2013;497(7448):249–253.

**6.** Ebelt H, Zhang Y, Kampke A, et al. E2F2 expression induces proliferation of terminally differentiated cardiomyocytes in vivo. *Cardiovasc Res*. 2008;80(2):219–226.

**7.** Porrello ER, Mahmoud AI, Simpson E, et al. Transient regenerative potential of the neonatal mouse heart. *Science*. 2011;331(6020):1078–1080.

**8.** Eulalio A, Mano M, Dal Ferro M, et al. Functional screening identifies miRNAs inducing cardiac regeneration. *Nature*. 2012;492(7429):376–381.

**9.** Braga L, Ali H, Secco I, Giacca M. Non-coding RNA therapeutics for cardiac regeneration. *Cardiovasc Res*. 2021;117(3):674–693.

**10.** Tian Y, Liu Y, Wang T, et al. A microRNA-Hippo pathway that promotes cardiomyocyte proliferation and cardiac regeneration in mice. *Sci Transl Med*. 2015;7(279):279ra38. https://doi.org/10.1126/scitranslmed.3010841

**11.** Borden A, Kurian J, Nickoloff E, et al. Transient introduction of miR-294 in the heart promotes cardiomyocyte cell cycle reentry after injury. *Circ Res*. 2019;125(1):14–25.

**12.** Chen J, Huang Z-P, Seok HY, et al. mir-17-92 cluster is required for and sufficient to induce cardiomyocyte proliferation in postnatal and adult hearts. *Circ Res*. 2013;112(12):1557–1566.

**13.** Gao F, Kataoka M, Liu N, et al. Therapeutic role of miR-19a/19b in cardiac regeneration and protection from myocardial infarction. *Nat Commun*. 2019;10(1):9530. https://doi.org/10.1038/S41467-019-09530-1

**14.** Torrini C, Cubero RJ, Dirkx E, et al. Common regulatory pathways mediate activity of micrornas inducing cardiomyocyte proliferation. *Cell Rep*. 2019;27(9):2759. https://doi.org/10.1016/J.CELREP.2019.05.005

**15.** Ali H, Braga L, Giacca M. Cardiac regeneration and remodelling of the cardiomyocyte cytoarchitecture. *FEBS J*. 2020;287(3):417–438.

**16.** Lesizza P, Prosdocimo G, Martinelli V, Sinagra G, Zacchigna S, Giacca M. Single-dose intracardiac injection of pro-regenerative microRNAs improves cardiac function after myocardial infarction. *Circ Res*. 2017;120(8):1298–1304.

**17.** Gabisonia K, Prosdocimo G, Aquaro GD, et al. MicroRNA therapy stimulates uncontrolled cardiac repair after myocardial infarction in pigs. *Nature*. 2019;569(7756):418–422.

**18.** Arsic N, Zacchigna S, Zentilin L, et al. Vascular endothelial growth factor stimulates skeletal muscle regeneration in vivo. *Mol Ther*. 2004;10(5):844–854.

**19.** Slavin GS, Saranathan M. FIESTA-ET: high-resolution cardiac imaging using echo-planar steady-state free precession. *Magn Reson Med*. 2002;48(6):934–941.

**20.** Chan RH, Maron BJ, Olivotto I, et al. Prognostic value of quantitative contrast-enhanced cardiovascular magnetic resonance for the evaluation of sudden death risk in patients with hypertrophic cardiomyopathy. *Circulation*. 2014;130(6):484–495.

**21.** Schmidt A, Azevedo CF, Cheng A, et al. Infarct tissue heterogeneity by magnetic resonance imaging identifies enhanced cardiac arrhythmia susceptibility in patients with left ventricular dysfunction. *Circulation*. 2007;115(15):2006–2014.

**22.** Simioniuc A, Campan M, Lionetti V, et al. Placental stem cells pre-treated with a hyaluronan mixed ester of butyric and retinoic acid to cure infarcted pig hearts: a multimodal study. *Cardiovasc Res*. 2011;90(3):546–556.

**23.** Lionetti V, Guiducci L, Simioniuc A, et al. Mismatch between uniform increase in cardiac glucose uptake and regional contractile dysfunction in pacing-induced heart failure. *Am J Physiol Heart Circ Physiol*. 2007;293(5):H2747–H2756.

**24.** Koch KC, vom Dahl J, Wenderdel M, et al. Myocardial viability assessment by endocardial electroanatomic mapping: comparison with metabolic imaging and functional recovery after coronary revascularization. *J Am Coll Cardiol*. 2001;38(1):91–98.

**25.** Bogaert J, Rademakers FE. Regional nonuniformity of normal adult human left ventricle. *Am J Physiol Heart Circ Physiol*. 2001;280(2):H610–H620.

**26.** Buxton AE, Lee KL, Fisher JD, Josephson ME, Prystowsky EN, Hafley G. A randomized study of the prevention of sudden death in patients with coronary artery disease. Multicenter Unsustained Tachycardia Trial Investigators. *N Engl J Med*. 1999;341(25):271–273. https://doi.org/10.1056/NEJM199912163412503

**27.** Buxton AE, Fisher JD, Josephson ME, et al. Prevention of sudden death in patients with coronary artery disease: the Multicenter Unsustained Tachycardia Trial (MUSTT). *Prog Cardiovasc Dis*. 1993;36(3):215–226.

**28.** Haim M, Strasberg B. Programmed ventricular stimulation: how low (with the coupling interval) and aggressive (with the protocol) should we go? No easy answers. *Isr Med Assoc J*. 2009;11(9):552–554.

**29.** Buxton AE, Lee KL, Fisher JD, Josephson ME, Prystowsky EN, Hafley G. A randomized study of the prevention of sudden death in patients with coronary artery disease. Multicenter Unsustained Tachycardia Trial Investigators. *N Engl J Med*. 1999;341(25):1882–1890. https://doi.org/10.1056/NEJM199912163412503

**30.** Richardson WJ, Clarke SA, Quinn TA, Holmes JW. physiological implications of myocardial scar structure. *Compr Physiol*. 2015;5(4):1877–1909.

**31.** Grabner W, Pfitzer P. Number of nuclei in isolated myocardial cells of pigs. *Virchows Arch B Cell Pathol*. 1974;15(4):279–294.

**32.** Lindsey ML, Zamilpa R. Temporal and spatial expression of matrix metalloproteinases and tissue inhibitors of metalloproteinases following myocardial infarction. *Cardiovasc Ther*. 2012;30(1):31–41.

**33.** Dewald O, Ren G, Duerr GD, et al. Of mice and dogs: species-specific differences in the inflammatory response following myocardial infarction. *Am J Pathol*. 2004;164(2):665–677.

**34.** Marmor A, Geltman EM, Schechtman K, Sobel BE, Roberts R. Recurrent myocardial infarction: clinical predictors and prognostic implications. *Circulation*. 1982;66(2):415–421.

**35.** Frangogiannis NG. The inflammatory response in myocardial injury, repair, and remodelling. *Nat Rev Cardiol*. 2014;11(5):255–265.

**36.** Senyo SE, Steinhauser ML, Pizzimenti CL, et al. Mammalian heart renewal by pre-existing cardiomyocytes. *Nature*. 2013;493(7432):433–436.

**37.** Beltrami AP, Urbanek K, Kajstura J, et al. Evidence that human cardiac myocytes divide after myocardial infarction. *N Engl J Med*. 2001;344(23):1248–1249.

**38.** González-Rosa JM, Martín V, Peralta M, Torres M, Mercader N. Extensive scar formation and regression during heart regeneration after cryoinjury in zebrafish. *Development*. 2011;138(9):1663–1674.

**39.** Leach JP, Heallen T, Zhang M, et al. Hippo pathway deficiency reverses systolic heart failure after infarction. *Nature*. 2017;550(7675):260–264.

**40.** Diez-Cuñado M, Wei K, Bushway PJ, et al. miRNAs that induce human cardiomyocyte proliferation converge on the Hippo pathway. *Cell Rep*. 2018;23(7):2168–2174.

**41.** Daubert JP, Zareba W, Hall WJ, et al. Predictive value of ventricular arrhythmia inducibility for subsequent ventricular tachycardia or ventricular fibrillation in Multicenter Automatic Defibrillator Implantation Trial (MADIT) II patients. *J Am Coll Cardiol*. 2006;47(1):98–107.

**42.** Mittal S, Hao SC, Iwai S, et al. Significance of inducible ventricular fibrillation in patients with coronary artery disease and unexplained syncope. *J Am Coll Cardiol*. 2001;38(2):371–376.

**43.** Antzelevitch C, Yan GX, Ackerman MJ, et al. J wave syndromes consensus conference: emerging concepts & gaps in knowledge. *Heart Rhythm*. 2016;13(10):e295. https://doi.org/10.1016/J.HRTHM.2016.05.024

**44.** Ruozi G, Bortolotti F, Mura A, et al. Cardioprotective factors against myocardial infarction selected in vivo from an AAV secretome library. *Sci Transl Med*. 2022;14(660):eabo0699. https://doi.org/10.1126/SCITRANSLMED.ABO0699

**45.** Zhang H, Li S, Zhou Q, et al. Qiliqiangxin attenuates phenylephrine-induced cardiac hypertrophy through downregulation of miR-199a-5p. *Cell Physiol Biochem*. 2016;38(5):1743–1751.

**46.** Song XW, Li Q, Lin LI, et al. MicroRNAs are dynamically regulated in hypertrophic hearts, and miR-199a is essential for the maintenance of cell size in cardiomyocytes. *J Cell Physiol*. 2010;225(2):437–443.

**47.** Li Z, Song Y, Liu L, et al. miR-199a impairs autophagy and induces cardiac hypertrophy through mTOR activation. *Cell Death Differ*. 2017;24(7):1205–1213.

**48.** El Azzouzi H, Leptidis S, Dirkx E, et al. The hypoxia-inducible microRNA cluster miR-199a∼214 targets myocardial PPARδ and impairs mitochondrial fatty acid oxidation. *Cell Metab*. 2013;18(3):341–354.

**49.** Wang S, Xie F, Chu F, et al. YAP antagonizes innate antiviral immunity and is targeted for lysosomal degradation through IKKε-mediated phosphorylation. *Nat Immunol*. 2017;18(7):733–743.

**50.** Huntington J, Pachauri M, Ali H, Giacca M. RNA interference therapeutics for cardiac regeneration. *Curr Opin Genet Dev*. 2021;70:48–53.

**KEY WORDS** gene therapy, heart, infarct, magnetic resonance, microRNA

**APPENDIX** For supplemental figures and tables, please see the online version of this paper.